SUPPLEMENTARY INFORMATION

LRAT-specific domain facilitates Vitamin A metabolism by domain swapping in HRASLS

Marcin Golczak[1*], Avery E. Sears[1], Philip D. Kiser[1], and Krzysztof Palczewski[1*]

From the [1]Department of Pharmacology, Cleveland Center for Membrane and Structural Biology, School of Medicine, Case Western Reserve University, Cleveland, Ohio 44106

[*]To whom correspondence may be addressed: Dept. of Pharmacology, School of Medicine, Case Western Reserve University, 10900 Euclid Ave., Cleveland, OH 44106. Tel.: 216-368-3063; Fax: 216-368-1300; E-mail: mxg149@case.edu.

[*]To whom correspondence may be addressed: Dept. of Pharmacology, School of Medicine, Case Western Reserve University, 10900 Euclid Ave., Cleveland, OH 44106. Tel.: 216-368-4631; Fax: 216-368-1300; E-mail: kxp65@case.edu.

SUPPLEMENTARY RESULTS

	HRASLS3/LRAT
Data collection	
Space group	$P4_32_12$
Cell dimensions	
a, *b*, *c* (Å)	63.12, 63.12, 157.97
α, β, γ (°)	90, 90, 90
Resolution (Å)	49.31-2.20 (2.33-2.20)[1,2]
R_{sym} (%)	5.4 (89.2)[2]
$I / \sigma I$	15.4(1.1)[2]
Completeness (%)	98.5(94.3)[2]
Redundancy	5.1(3.3)[2]
Refinement	
Resolution (Å)	49.30-2.20
No. reflections	15934
R_{work} / R_{free} (%)	20.7/24.8
No. atoms	2243
Protein	2167
Ligand/ion	16
Water	60
B-factors (Å^2)	
Protein	64.0
Ligand/ion	53.0
Water	58.0
R.m.s. deviations	
Bond lengths (Å)	0.014
Bond angles (°)	1.68

[1]Reported data set was collected on a single crystal.
[2]Highest-resolution shell is shown in parentheses.

Supplementary Table 1 – X-ray data collection and refinement statistics.

Supplementary Figure 1 – *Sequence alignment of LRAT and HRASLS proteins.* Sequences of human HRASLS2–4 and LRAT were aligned by using ClustalW2 available at the EMBL-EBI server. Conserved His residues and six amino acid stretches containing the catalytic Cys residue are highlighted in red, whereas the predicted C-terminal transmembrane segments are shown with a gray background. The stretch of LRAT sequence used to construct the HRASLS/LRAT chimeric proteins is shown with a green background. Mutations within the LRAT sequence associated with severe retinal dystrophies are marked with blue. The secondary structure diagrams are placed based on the crystal structure of HRASLS3 (PDB accession 4DOT).

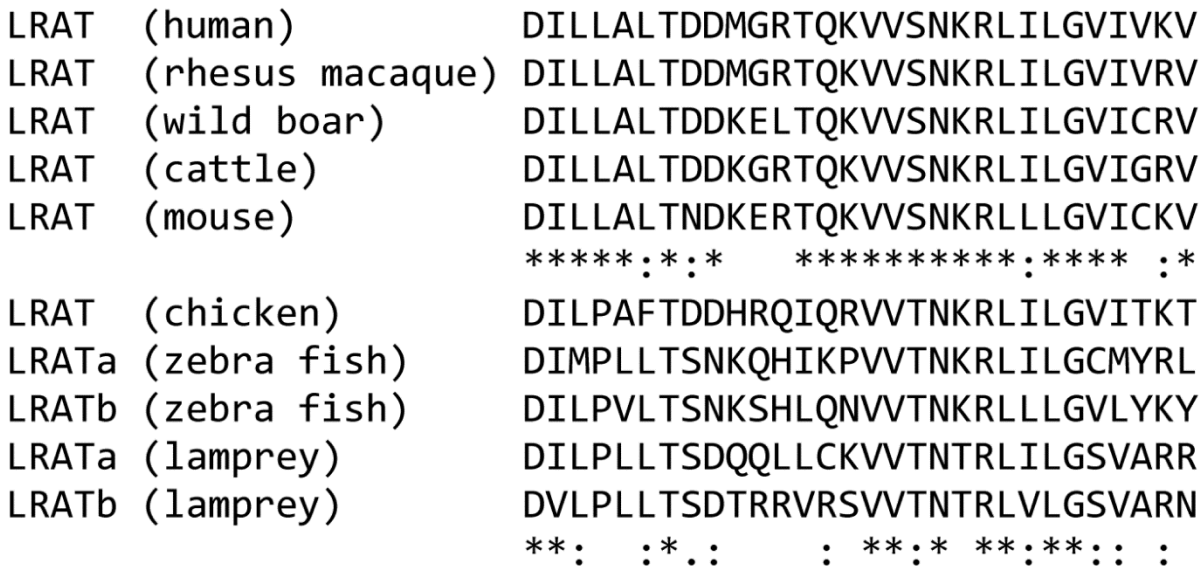

Supplementary Figure 2 – *Sequence alignment of LRAT-specific domain.* The 30-aa sequence characteristic for LRAT is highly conserved across multiple species. It is also present in the Lamprey ortholog of LRAT, the evolutionary oldest enzyme that catalyzes phospholipid-dependent retinyl ester formation.

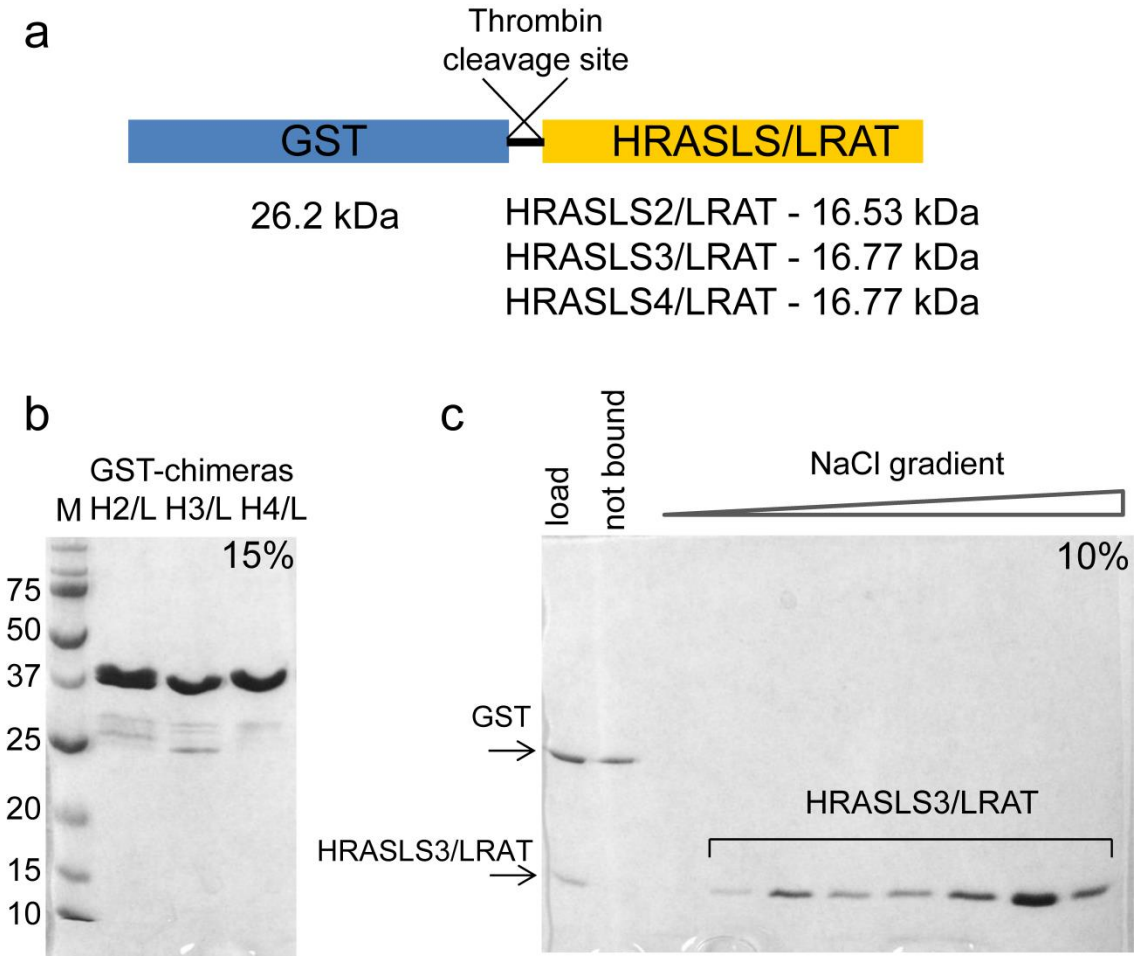

Supplementary Figure 3 – *Purification of HRASLS/LRAT chimeric proteins.* (**a**) Schematic representation of GST-fused chimeric enzymes expressed in *E. coli*. The molecular mass of these chimeric proteins includes N-terminal GS sequences, part of the thrombin cleavage site and a C-terminal EFIVTD cloning artefact. (**b**) SDS-PAGE of HRASLS/LRAT proteins after glutathione affinity column purification. (**c**) HRASLS3/LRAT after GST tag cleavage and final purification on a SP-sepharose column. The gel was stained with Coomassie Blue R-250. Single protein bands indicate the high purity of this protein preparation.

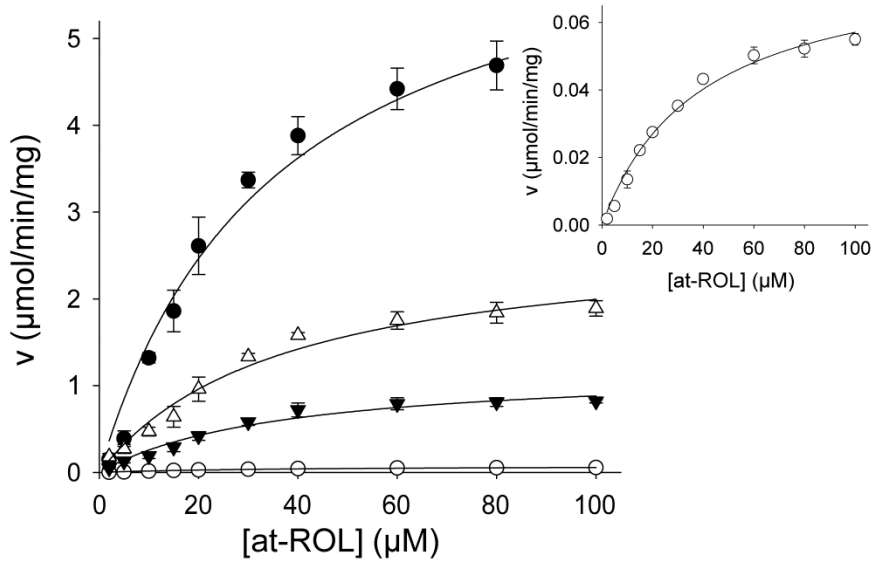

Enzyme	K_M (µM)	V_{max} (µmol/min/mg)	K_d (µM)
GST-tLRAT	35.4 ± 6.2	6.83 ± 0.51	0.20 ± 0.05
HRALSL2/LRAT	36.7 ± 7.8	1.21 ± 0.11	0.18 ± 0.03
HRALSL3/LRAT	38.7 ± 5.5	0.08 ± 0.01	0.26 ± 0.06
HRASLS4/LRAT	36.9 ± 6.8	2.73 ± 0.22	0.28 ± 0.05

Supplementary Figure 4 – Kinetics of the all-*trans*-retinol esterification reaction. The relationship between the initial velocity of the enzymatic reaction and all-*trans*-retinol concentration was fitted with the Michaelis-Menten kinetic model. Symbols correspond to GST-tLRAT (●), HRASLS4/LRAT (Δ), HRASLS2/LRAT (▼), and HRASLS3/LAT (○). The inset represents a graph for HRASLS3/LRAT. Kinetic parameters of retinyl ester formation and all-*trans*-retinol binding constants for LRAT and HRASLS/LRAT chimeric proteins calculated based on fluorescence assay (Fig. 2c) are listed in a table. Standard deviations of the mean value for three independent experiments are provided.

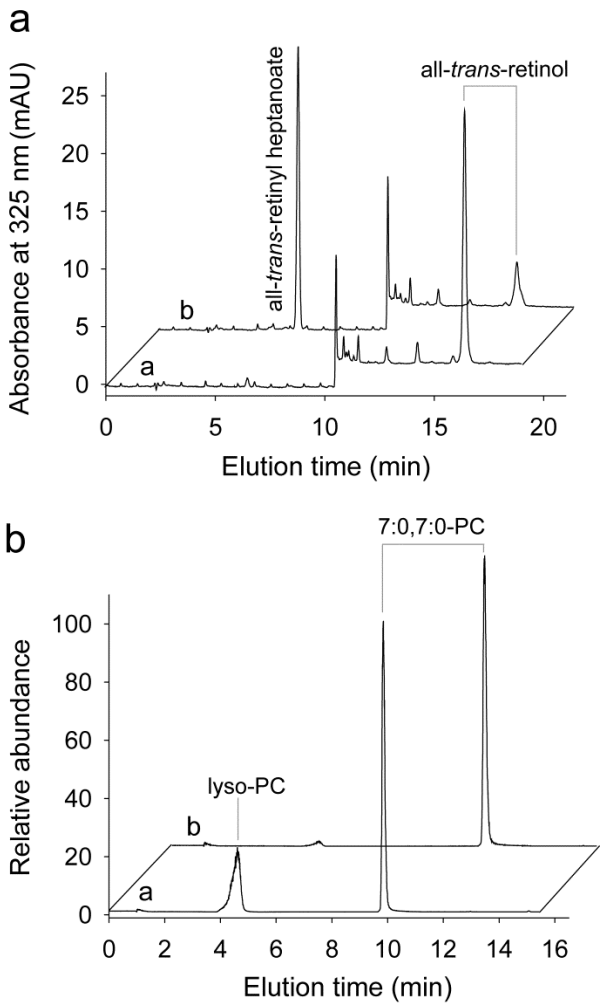

Supplementary Figure 5 – *Enzymatic activity of the LRAT deletion mutant.* (**a**) Production of retinyl esters was virtually absent after incubation with the LRAT deletion mutant in which the 30-aa linker between the β3 and β4 strands was trimmed to leave only a short sequence of polar residues (NDKERTQK). Chromatogram "a" corresponds to the sample incubated with the mutated enzyme, whereas "b" represents GST-tLRAT as a positive control. (**b**) Hydrolysis of 7:0, 7:0-PC by the LRAT mutant. Although all-*trans*-retinol esterification was compromised, the mutated enzyme retained the ability to cleave a phospholipid substrate. Chromatograms represent ion intensities for m/z = 482.3 $[MH]^+$ (phospholipid substrate) and 370.3 $[MH]^+$ (lyso-PC products). Traces "a" and "b" represent samples incubated with or without the mutated enzyme, respectively.

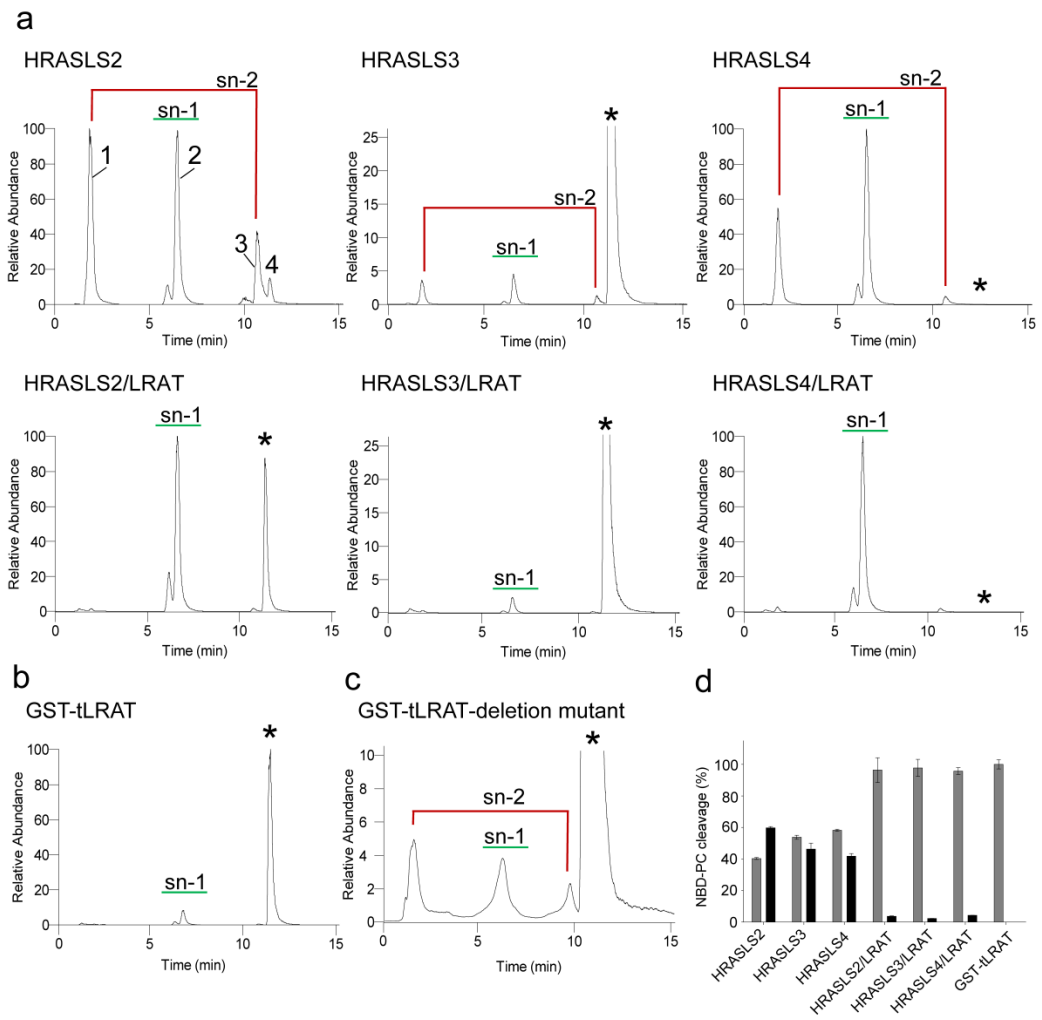

Supplementary Figure 6 – *Sn-1/sn-2 specificity of HRASLS2, 3 and 4 and their corresponding chimeric enzymes.* The preferred site of ester bond hydrolysis in PC was determined by using a PC substrate labeled with the NBD chromophore at the sn-2 position (NBD-PC). (**a**) HRASLS enzymes (5 µg) incubated with 0.1 mM NBD-PC in the presence of 5% methanol yielded products characteristic of both sn-1 and sn-2 ester bond cleavage as detected by LC/MS. Like LRAT (**b**) but in contrast to the native proteins, the chimeras preferentially cleaved phospholipids at the sn-1 position. Asterisks indicate the eluted substrate. (**c**) Regio-specificity of PC cleavage by the LRAT deletion mutant. Incubation of the deletion mutant with NBD-PC revealed both sn-1 and sn-2 phospholipid cleavage products indicating lack of sn-1 site specificity characteristic of the native enzyme [1] or GST-tLRAT. (**d**) Products of sn-1 (1-hydroxy-2-hexanoyl-NBD-lyso-PC) and sn-2 (6-NBD-hexanoic acid methyl ester) cleavage were quantified based on the characteristic absorbance spectrum of the NBD chromophore after separation by HPLC. Chromatographic separation, MS identification, and UV/Vis-based quantification of the substrate and products used in this enzymatic assay are shown in Supplementary Fig. 7. Data represent mean values from two independent experiments performed in triplicate ± s.d. MS-based identification of NBD-PC cleavage products is presented in Supplementary Fig. 7.

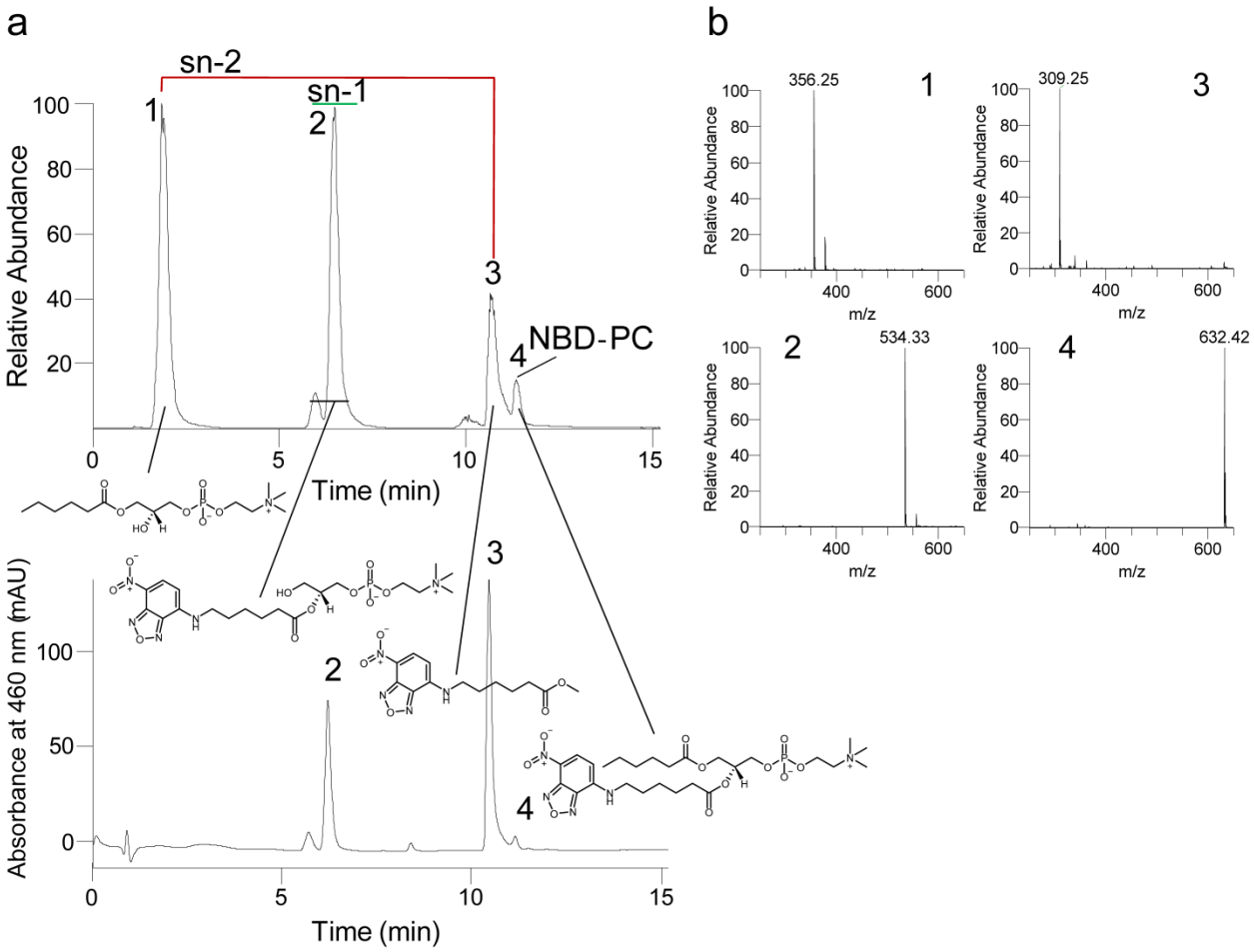

Supplementary Figure 7 – *HPLC separation and detection of the enzymatic cleavage products of NBD-PC.* The preferential site of ester bond hydrolysis in PC was determined by using a phospholipid substrate labeled with NBD chromophore at the sn-2 position. (**a**) Incubation of HRASLS protein with NBD-PC under standard conditions used for the lipolysis assay but in the presence of 5% methanol yielded three separate reaction products readily detected by MS (top panel). Two of these products revealed a characteristic absorbance for the NBD chromophore and thus could be detected and quantified based on UV/Vis absorbance at 460 nm (bottom panel). Based on the molecular masses (shown in panel **b**), peak 1 corresponded to 1- hexanoyl-2-hydroxy-lyso-PC, peak 2 to 1-hydroxy-2-hexanoyl-NBD-lyso-PC, and peak 3, the hexanoyl-NBD methyl ester. Peak 4 was assigned to the remaining substrate. Thus, peaks 1 and 3 represent products of the sn-2 cleavage, whereas peak 2 signifies liberation of the acyl moiety from the sn-1 position of the phospholipid substrate.

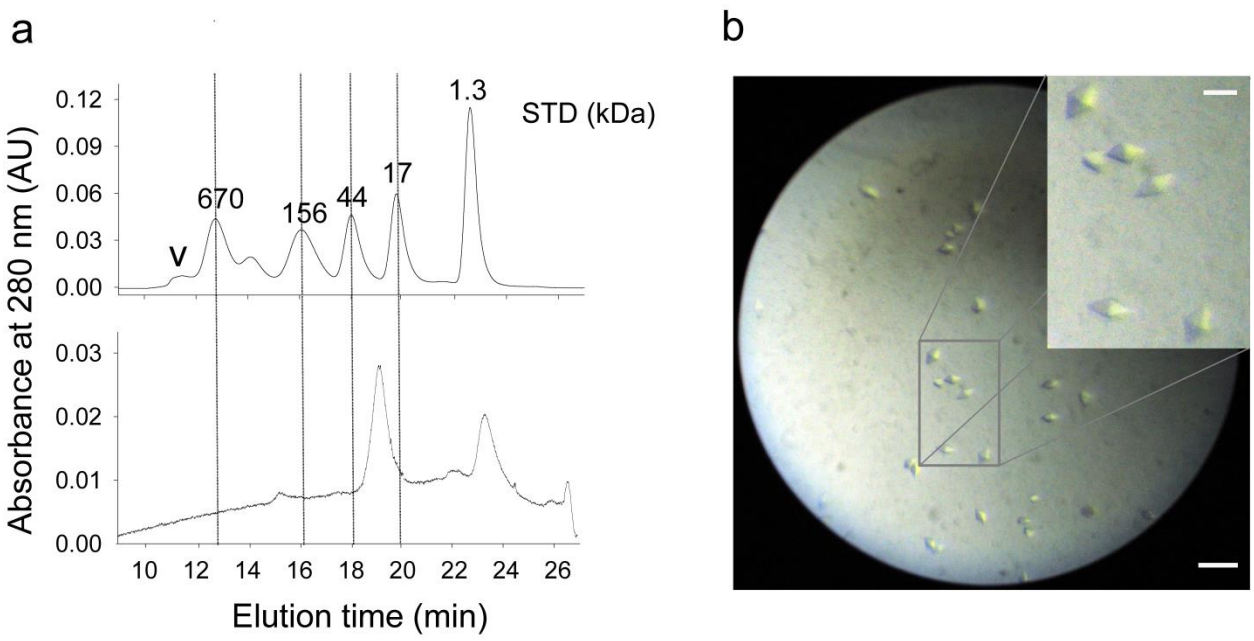

Supplementary Figure 8 – *Oligomerization and crystal formation of the HRASLS3/LRAT chimeric protein.* (**a**) Gel filtration of the purified protein. One mg of HRASLS3/LRAT was loaded onto a Superdex 200 (10/300) column (Pharmacia) equilibrated with 20 mM Tris/HCl buffer, pH 8.0, containing 5 mM DTT. By comparison to protein standards (top panel), the elution profile of HRASLS3/LRAT indicates that this protein formed a dimer in solution (bottom panel). (**b**) Crystals of HRASLS3/LRAT grown in the presence of 5 mM 7:0,7:0-PC and 0.1 M Tris/HCl, pH 8.5, 0.2 M NaCl, and 20% (w/v) polyethylene glycol 3350. Bars correspond to 150 µm in the main picture and 50 µm in the zoomed inset.

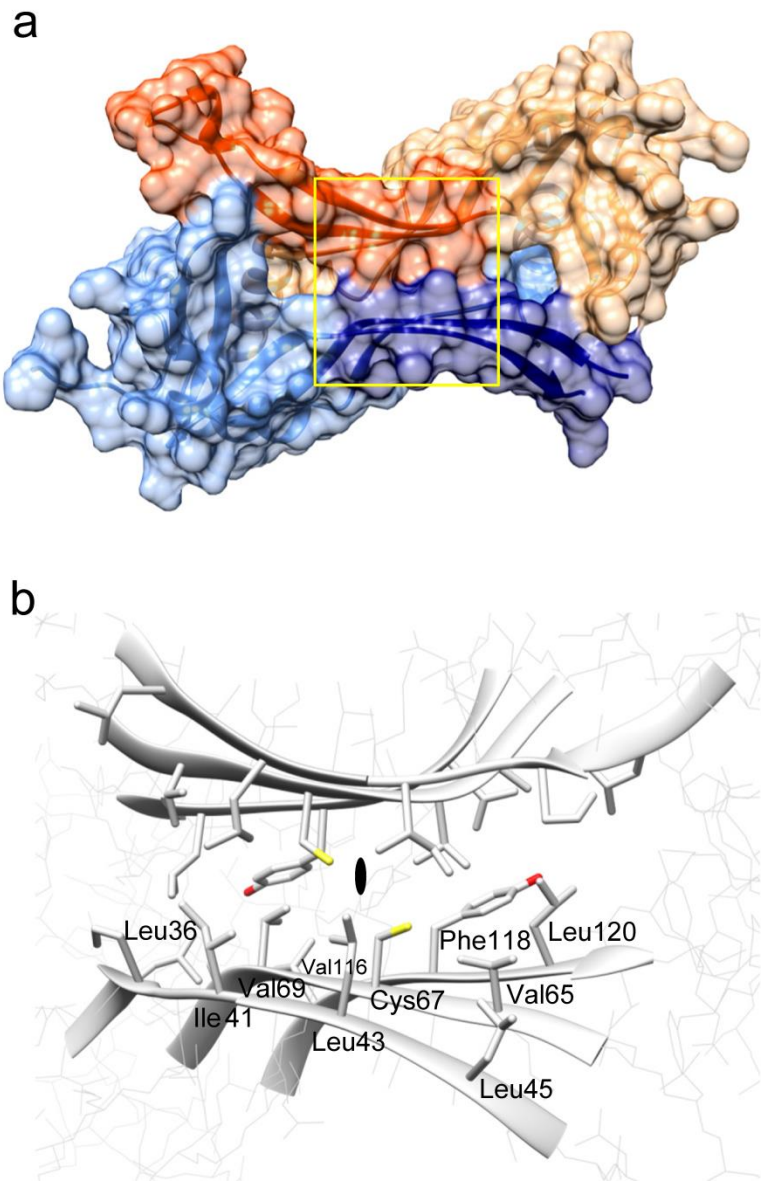

Supplementary Figure 9 – *LRAT-specific domain contribution to the dimerization interface.* (**a**) Molecular surface of the HRASLS3/LRAT dimer. Positions of LRAT domains are represented with red and dark blue colors. Yellow rectangle marks an area of hydrophobic interaction between the protomers detailed in panel B. (**b**) Hydrophobic interactions between two neighboring β-sheets formed with a dominant contribution of the LRAT domain. The center of the dimer symmetry is marked by a symbol marking the twofold axis perpendicular to the plane of the figure.

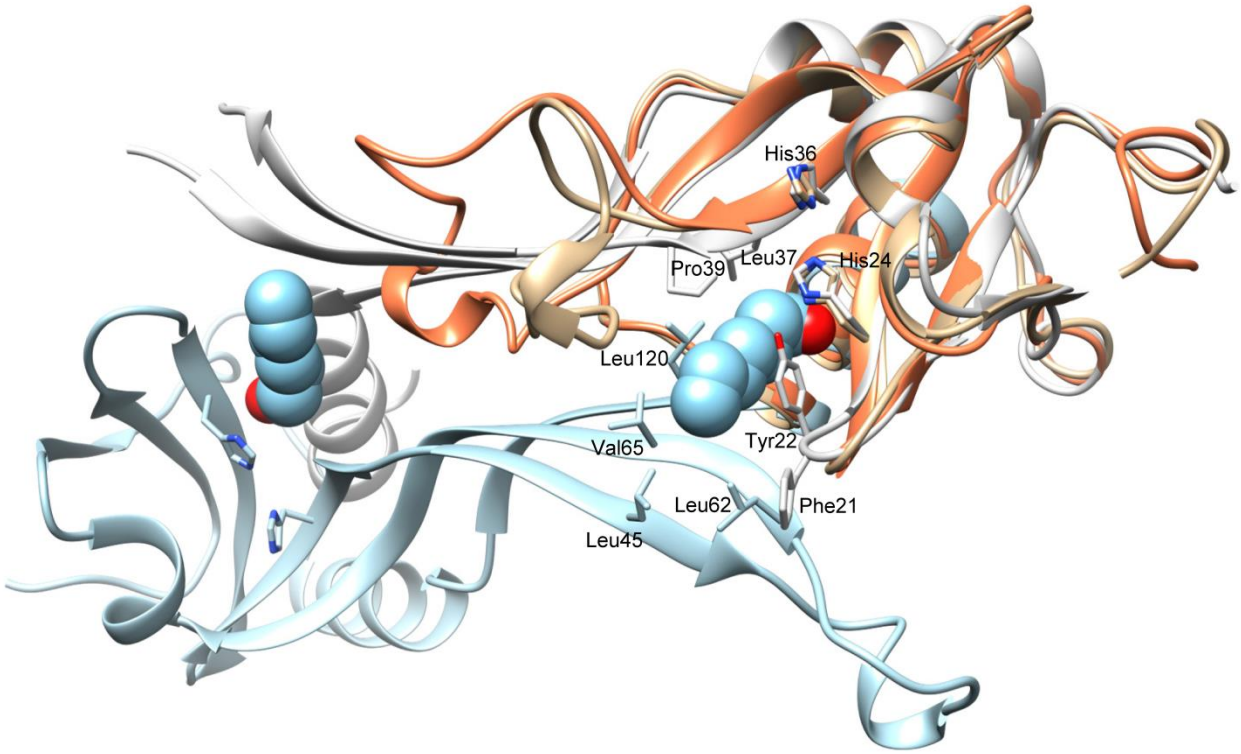

Supplementary Figure 10 – *Structural comparison of HRASLS3 and the HRASLS3/LRAT chimera.* Two NMR structures of native HRASLS3, shown in coral and sandy brown colors (PDB accession 2KYT) [2] that differ in the conformation of a flexible linker between β-strands 3 and 4 of the catalytic domain were superimposed with that of the HRASLS3/LRAT chimera (colored light blue and gray). Key catalytic side chains as well as residues forming a hydrophobic pocket in the chimeric enzymes are indicated. The thioester C-7 acyl moiety is shown in spheres. This figure clearly demonstrates a difference in the active site environment between the native and chimeric enzymes and also reveals the structural organization of the pocket surrounding the acyl moiety.

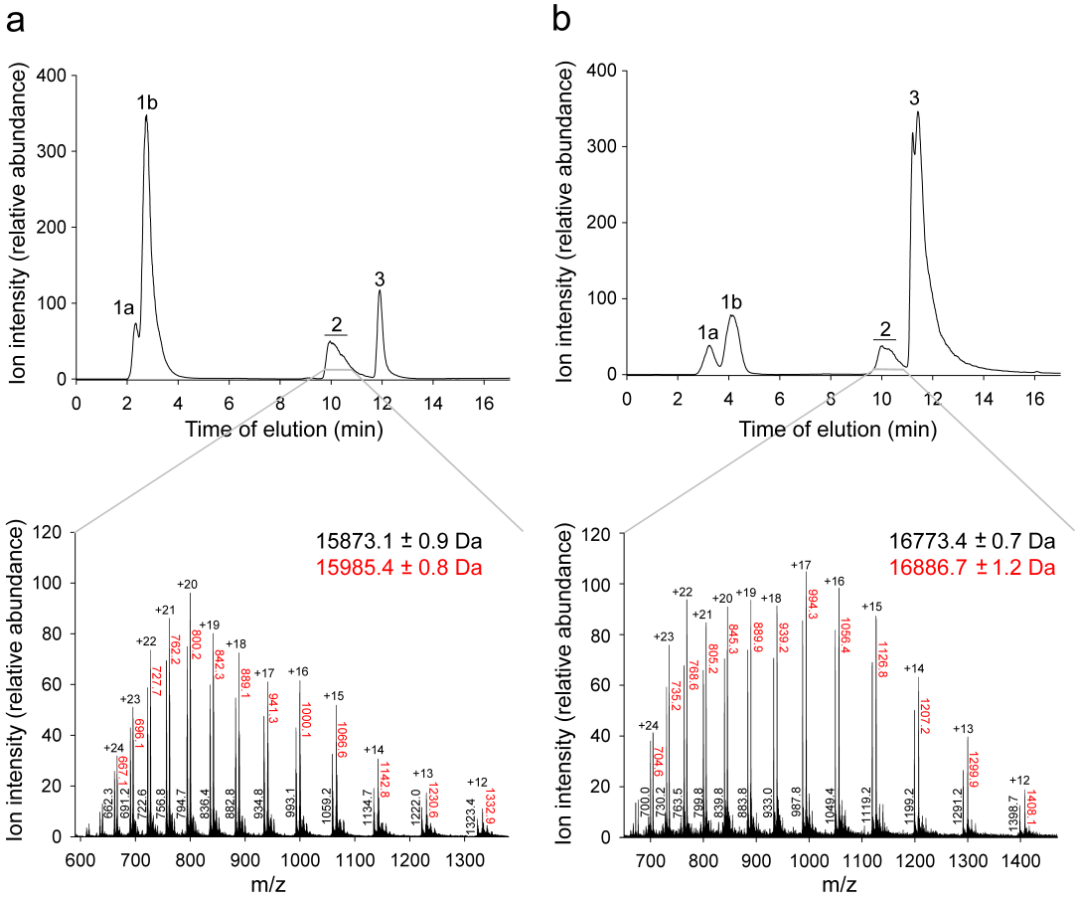

Supplementary Figure 11 – *Self-acylation of HRASLS3 and HRASLS3/LRAT chimera in the presence of a phospholipid substrate*. One µg of each protein was incubated with 1 mM 7:0,7:0-PC in 10 mM Tris/HCl, pH 8.0, 1 mM DTT for 20 min at 25 °C. The mixture was then analyzed by LC/MS. Panels (**a**) and (**b**) represent the chromatographic separation (top) and MS spectra (bottom) of intact HRASLS3 and its corresponding chimeric protein, respectively. Peaks 1a and 1b correspond to the lyso-PC products and indicate a preferential intramolecular acyl shift from the sn-2 to the sn-1 position. The broad peak 2 corresponds to intact protein, whereas peak 3 represents the phospholipid substrate. The MS spectra display two groups of multiply-charged protein ions that correspond to the unmodified and acylated forms of these proteins. Deconvolution of the HRASLS3 and HRASLS3/LRAT chimera spectra revealed protein masses of 15,873 Da and 16,773 Da, which are virtually identical (with respect to measurement error) to the theoretical masses of the recombinant enzymes. Incubation with 7:0,7:0-PC led to a ~112-Da shift in the experimentally obtained protein masses as calculated from the additional series of ions present in the MS spectra (labeled in red). This mass difference matches that of a heptanoic acid moiety carried by the phospholipid substrate.

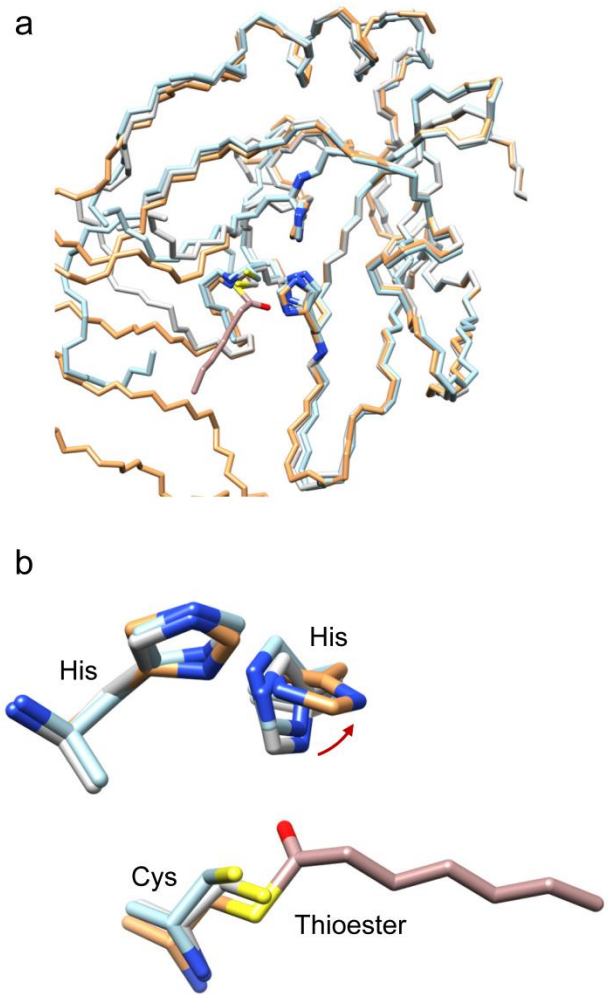

Supplementary Figure 12 – *Changes in the active site architecture upon enzymatic self-acylation.* (**a**) Alignment of the polypeptide chains of HRASLS2 (light blue, PDB accession 4DPZ) [3], HRASLS3 (gray, PDB accession 4DOT) [3] with the acylated form of HRASLS3/LRAT chimeric protein (light orange). RMSD values of 0.75 (back bone) and 1.22 (all atoms) for HRASLS3 and 0.58 and 1.21, respectively for HRASLS2 indicate no significant differences between these structures. However, acylation of the Cys residue in the active site provokes ~80˚ rotation of the imidazole side chain in the adjacent catalytic His to avoid an unfavorable clash of $N^{\delta 1}$ atom with the thioester carbonyl oxygen. (**b**) Changes in the orientation of the His side chain could have functional significance by enabling deprotonation of the hydroxyl group of an acyl acceptor. Calculations of RMSD were done with SuperPose server [4].

Supplementary Movie – *Structural organization of the active site in HRASLS3/LRAT chimeric enzyme.* This movie demonstrates structural differences between the native and chimeric enzymes in its acylated state. The architecture of the active site in HRASLS3/LRAT chimera is determined by hydrophobic residues that formed an envelope around the key residues involved in catalysis. Side chain of these aa as well as residues forming a hydrophobic pocket are indicated. The thioester C-7 acyl moiety is shown in spheres. Structures of native HRASLS3 is shown in sandy brown colors (PDB accession 2KYT).

References

1. MacDonald, P.N. & Ong, D.E. A lecithin:retinol acyltransferase activity in human and rat liver. *Biochem Biophys Res Commun* **156**, 157-63 (1988).
2. Ren, X., Lin, J., Jin, C. & Xia, B. Solution structure of the N-terminal catalytic domain of human H-REV107--a novel circular permutated NlpC/P60 domain. *FEBS Lett* **584**, 4222-6 (2010).
3. Golczak, M. et al. Structural basis for the acyltransferase activity of lecithin:retinol acyltransferase-like proteins. *J Biol Chem* **287**, 23790-807 (2012).
4. Maiti, R., Van Domselaar, G.H., Zhang, H. & Wishart, D.S. SuperPose: a simple server for sophisticated structural superposition. *Nucleic Acids Res* **32**, W590-4 (2004).